Tumor Uptake as a Function of Tumor Mass: A Mathematic Model

Lawrence E. Williams, Rosemary B. Duda, Richard T. Proffitt, Barbara G. Beatty, J. David Beatty, Jeffrey Y.C. Wong, John E. Shively, and Raymond J. Paxton

Divisions of Radiology, Surgery and Immunology at the City of Hope National Medical Center, Duarte; and Vestar Inc., Pasadena, California

Inverse correlations of tumor uptake (u), measured in percent injected dose per gram, with tumor mass (m) are demonstrated for phospholipid vesicle, nonspecific and specific monoclonal antibody tracers. Correlation coefficients implied $u = B\ m^A$ in 11 different animal experiments. Experimental exponent (A) values lay in the range −0.28–0.64 with a mean of −0.43 while intercept (B) values varied from 3 to 18. Spherical and cylindrical tumor models implied exponents of −0.33 and −0.5, respectively. Comparison of three implantation sites of the human LS174T xenograft revealed a narrow range of exponents (−0.38–−0.46) indicating a consistent geometry for this tumor. Blood flow to the lesion site and inside its volume (as dictated by tumor size) are factors in tumor uptake. Our results indicate that biodistribution data should include the variation of tumor uptake with mass. For <10 g lesions, we predict that radiation absorbed dose will be highly dependent upon tumor size.

J Nucl Med 29:103–109, 1988

A number of recent reports involving animal models have noted the variation of tumor uptake of radiotracers as a function of tumor size. Patel et al. (*1*), using indium-111- (^{111}In) labeled phospholipid vesicles, demonstrated a decrease of uptake (u), measured in percent injected dose per gram of tumor (%ID/g), as the mass (m) of sub-cutaneous (SC) Lewis Lung Carcinoma (LLC) increased. In a similar liposome study by Ogihara et al. (*2*), uptake of encapsulated gallium-67 (^{67}Ga) by rat Yoshida sarcoma was shown to decrease with tumor size. Both experimental groups utilized long chain phospholipids in the artificial membranes so as to ensure thermal stability in vivo (*3*). Earlier vesicle biodistribution experiments, done with membranes of unknown integrity in blood, are probably not directly comparable to these results.

Labeled monoclonal antibodies (MAbs) have also been studied in the context of variation of uptake with tumor mass (*4,5*). Our group (*4*) had initially identified the decrease in the uptake of the T84.66 anti-CEA monoclonal antibody as the mass of LS174T, a CEA-producing human tumor xenograft, increased. A correlation between the logarithm of u and the logarithm of m was demonstrated in that tumor-specific example. More recently, Halpern and co-workers (*5*) have reported on both tumor-specific and nonspecific MAbs in human xenografts in the nude mouse. In the former case, an inverse correlation between uptake and mass was described, but not quantitated.

Earlier biodistribution results involving MAbs were somewhat equivocal with regard to mass effects. Moshakis et al. (*6*) described a qualitative decrease in the uptake of the specific monoclonal LICR-LON/HT13 as the mass of human germ cell tumor xenografts increased. Using a splenic-implant model, Shah et al. (*7*), reported similar results for the specific combination LS174T and B72.3. In addition, however, they found a second specific combination, the human Clouser tumor and B6.2 MAb, in which uptake was essentially independent of mass out to values as large as 1,000 mg. Autoradiographic studies revealed this tumor to contain a number of antigen-antibody complexes scattered throughout the lesion volume.

Inverse correlations between u and m are not surprising since the internal volume of a tumor is often found to be more poorly perfused as its size increases (*8*). Relatively large necrotic zones would be expected to be inaccessible to any blood-borne agent (*9*). What is required, however, is a mathematic picture of the tracer-tumor interaction which will predict the nature of the function u(m). If known, one could make better comparisons of one tumor uptake with another in

Received Feb. 4, 1987; revision accepted July 7, 1987

For reprints contact: L. E. Williams, Dept. of Radiology, City of Hope National Medical Center, Duarte, CA 91010.

quantitative terms and, correspondingly, improve calculations of radiation dose in therapeutic applications. In the following, we demonstrate the mathematic nature of the empirical correlations between uptake and mass and develop a theoretical picture of the tumor which is consistent with the majority of these correlations.

MATERIALS AND METHODS

Tracer Preparations

Only those vesicles made of long-chain synthetic phospholipids were included in our analysis (*3,10*). Neutral liposomes were ~60 nm in diameter and made of distearoyl phosphatidylcholine (DSPC) and cholesterol (CH) in a 2:1 molar combination (*1*). Radiolabeling with ^{111}In was done using the method of Mauk and Gamble (*11*). Positive liposomes were approximately the same size as the neutral and made with DSPC, CH, and stearylamine in a 10:5:1 ratio (*2*). Loading with gallium-67 (^{67}Ga) was accomplished with the method of Hwang et al. (*12*). Some of the results included here are taken directly from the literature (*1,2*), with additional data being provided on the targeting of neutral vesicles to the EMT6 murine tumor.

Monoclonal agents were produced by hybridoma technology and the appropriate bifunctional chelate labeling techniques have been extensively described (*13*). We have purposely omitted consideration of iodinated agents in this analysis in order to obviate problems of dehalogenation in vivo (*14*). Some of the antibody results included here are from the earlier literature (*4,5,7*). In addition, previously unpublished data from our studies involving intraperitoneal (i.p.) tumor implantation and i.v. as well as i.p. routes of MAb injection are included to demonstrate the general applicability of the correlations and mathematic model.

Organ Assay

Organs were prepared by euthanizing the animals, dissecting the lesions, and removing residual blood. Count rates were corrected for decay and divided by the initial injection dose rate as well as the tumor mass to provide the ratio of percent injected dose per gram. All biodistribution data were at times ≤ 24 hr in order to allow targeting (*15*).

Mathematic Correlations

First-order correlations were evaluated with the three standard forms being:

$$\text{linear } u = A\,m + B \qquad (1a)$$

$$\text{exponential } u = B \exp(A\,m) \qquad (1b)$$

and

$$\text{power law } u = B\,m^{A} \qquad (1c)$$

Because of the first-order assumption, the constants A and B represent unique values which were obtained using a least-squares minimization program. It is to be anticipated that these parameters are capable of physical interpretation if an appropriate model of tumor perfusion is considered. While no general model is possible due to the variation of lesion geometry, it is initially instructive to carry out a theoretic calculation based on a spherical representation of the smaller lesions.

Theoretic Model of the Tumor

Let us consider the spherical tumor of radius s shown in Figure 1A. We will assume a blood supply that is constrained to the lesion surface with an effective tracer penetration depth of d units. This depth is assumed to be independent of tumor mass, but dependent upon the tumor and tracer types. The latter assumption follows from the fact that membrane penetration and diffusion will greatly affect the actual distance to which the material can penetrate beyond the capillary wall. At depths beyond d the concentration of the tracer is set to

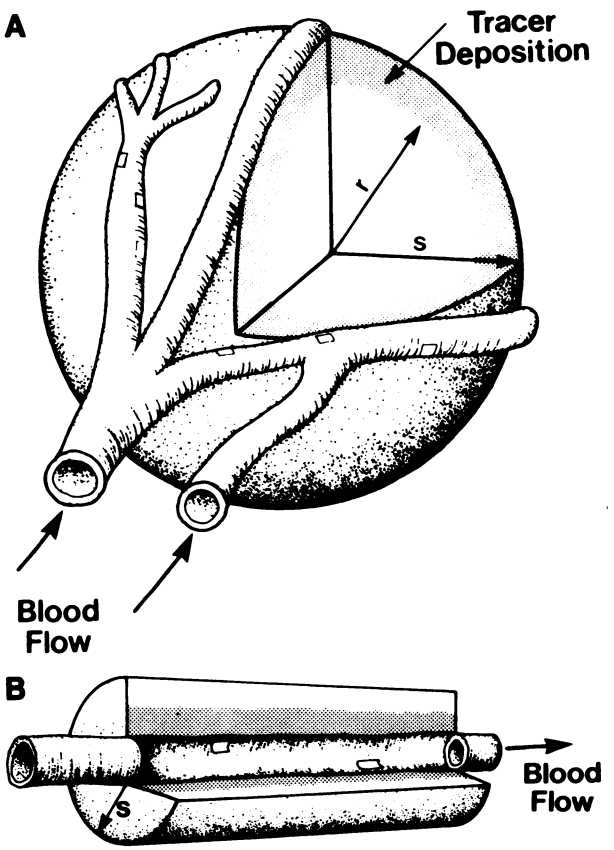

FIGURE 1
A: A cut-away schematic of a spherical tumor of radius s. Uniform tracer deposition is assumed in a shell of material having a thickness d. The inner radius of this shell is defined as r = s − d. Small openings (fenestrations) are indicated in the blood vessel walls. Regions of tracer deposition are shown by stippling. B: Cylindrical model of tumor development. As in the spherical case, the only neoplastic cells receiving tracer are those adjacent to the blood vessel. Growth occurs from the inside and outer cells become necrotic. The length of the cylindrical segment is fixed by the geometry of the blood vessel network and is independent of mass.

zero so that we are imagining an accessible spherical shell of thickness d = s − r lying on the surface of the lesion. Mathematically, we have:

$$u = \frac{\text{Amount of tracer in tumor (\%ID)}}{\text{Mass of tumor (g)}}. \quad (2)$$

In Eq. (2), we postulate that the numerator will be proportional to the perfusable volume while the denominator will be the product of the mass density and the lesion volume. Using the spherical shell picture, we find:

$$u = \frac{4/3\ \pi\ (s^3 - r^3)\ k}{4/3\ \pi\ D\ s^3}, \quad (3)$$

where D is the mass density and k is proportional to the density of binding sites for the tracer-target combination in question. Yet s − r is d so that the right side can be simplified by a power series expansion to yield:

$$u \cong (3\ k\ d)/D\ s = \text{constant}/s, \quad (4)$$

with the constant being 3 k d/D. One can relate s, the outer radius, to the mass by the expression shown in the denominator of Eq. (3) so that:

$$u = \text{constant}'/m^{1/3}. \quad (5)$$

In other words, the uptake is related, through terms of first order in d/s, to the inverse of the cube root of the mass.

This result is dependent upon the growth pattern of the lesion since a nonisotropic development would lead to a different exponent in Eq. (5). For example, a cylindrical tumor whose length is fixed so as to be independent of its mass; i.e., having only two degrees of freedom, would lead to a value of −0.5. This structure could arise if we consider the tumor to grow around a set of pre-existing capillaries as seen in Figure 1B. Here, the length of the resultant cylindrical lesion becomes fixed relatively early and only radial growth is permitted. The similarity between the results obtained with the spherical and cylindrical models and the power-law formula of Eq. (1C) can be noted.

The magnitude of d can be estimated (*16*) via a diffusion calculation based on the molecular weight of IgG molecules or the known size of the liposomes. This distance is on the order of 1 mm or less; i.e., somewhat below the smallest size lesions considered here.

RESULTS

Comparisons of sample results using the three different linear least squares possibilities are given in Table 1. In the first example involving vesicles and LLC in the BALB/c mouse (*1*), all three forms of the least squares algorithm give rise to correlations which are significant at the 1% level of confidence. The correlation coefficient (ρ) is greatest for the power-law formulation, however, having a value of −0.823. Negative correlation indicates the inverse nature of the relationship; the best-fit value of the exponent (A) being −0.28 in this case.

An example of a nonspecific protein studied by Hagan et al. (*5*) is shown in the table. Here, we demonstrate inverse correlations between the uptake of PSA-399 and lymphoma in the nude mouse. Both log-log and exponential models had correlations which were significant at the 5% level, although the linear correlation was not. Only the power-law correlation was significant at the 1% level of confidence, however, with the exponent being −0.49, a value somewhat larger than that seen above.

TABLE 1
Sample Correlations of Tumor Uptake with Mass

	Linear	Exponential	Power-Law	n*	Ref
	Vesicles (^{111}In) with Lewis lung CA				
A†	−5.81	−0.390	−0.278	20	1
B	18.8	17.9	10.6		
ρ	−0.617	−0.676	−0.823	[0.537]‡	
	PSA-399 (nonspecific Mab) with lymphoma				
A	−0.415	−0.134	−0.486	15	
B	4.46	3.82	0.93		
ρ	−0.314	−0.538	−0.807	[0.606]	5
	T-101 (specific Mab) with lymphoma				
A	−0.878	−0.165	−0.305	15	
B	8.68	8.45	1.70		
ρ	−0.723	−0.827	−0.882	[0.606]	5

* n is the number of data points.

† A is the slope, B the intercept of the three mathematic models listed. See text for details.

‡ Numbers in brackets are the ρ values at the 1% level of confidence.

The table also contains the comparable results for the case of experiments (*5*) involving the specific T-101 monoclonal and lymphoma in a nude mouse. While all correlation coefficient values were significant at the 1% level, the highest coefficient occurs for the log-log model of the u(m) relationship given by Eq. (1C). The exponential formulation gives rise to a fit which is almost as good, but the linear representation is again a somewhat poorer picture of the regression law. The slope of the fitted curve in the power-law case predicts that the exponent is −0.31.

Table 2 contains the summary of power-law correlations using the three vesicle and eight monoclonal data sets. All correlations were significant at the 1% level with several being significant at the 0.1% level. Slopes ranged from −0.28 to −0.64 with most values lying between −0.3 and −0.5. Because of the form of the power-law relationship, it is not possible to assign a unique set of dimensions to the B parameter. We have, therefore, omitted any units in the B column of Table 2. Calculation of uptakes are straightforward using the tabular values since each row is internally consistent so as to yield an uptake having units of %ID/g. We have included in the table u (0.1 g) to permit one comparison of the various tracer/tumor combinations. Alternatively, one may compare B parameters as a somewhat simplistic, but direct index of the accessibility of tumor receptor sites. The observed range of B values is between

TABLE 2
A Comparison of Power-Law Correlations of Tumor Uptake and Mass

Type	Tumor target	n	Slope (A)	Intercept (B)	ρ	u(0.1g)*	Ref
			Vesicle agents				
0 charge	Lewis lung	17	−0.28	10.6	−0.823	20.2	1
0 charge	EMT6	27	−0.64	15.1	−0.952	65.9	This study
+ charge	Rat sarcoma†	28	−0.42	5.35	−0.762	14.1	2
			Mab agents				
T-101	Lymphoma	15	−0.31	5.48	−0.882	11.2	5
PSA-399	Lymphoma	15	−0.49	2.53	−0.807	7.8	5
CEJ-326	T-380	16	−0.48	15.3	−0.821	46.2	5
9.2.27	Melanoma	18	−0.42	9.1	−0.775	23.9	5
			α-CEA Mabs				
B72.3 (IV)	LS174T (IS)	15	−0.39	11.8	−0.800	29.0	7
T84.66 (IV)	LS174T (SC)	17	−0.38	18.1	−0.740	43.4	This study
T84.66 (IV)	LS174T (IP)	46	−0.46	3.2	−0.546	9.1	This study
T84.66 (IP)	LS174T (IP)	51	−0.38	2.8	−0.372	6.8	This study

* u(0.1g) is the calculated uptake (% (ID/g) in a 0.1 g lesion.
† Rat uptake should be scaled upward to be compared with murine data.

2.5 and 18.1 with the lowest magnitude occurring for the nonspecific MAb PSA-399 and the lymphoma target. Maximum intercept corresponded to the specific anti-CEA MAbs T84.66 and the LS174T human colorectal tumor implanted subcutaneously.

Slope values obtained for the LS174T target were found to be −0.39 and −0.38 in the intrasplenic and subcutaneous implantation with i.v. injection of the tracer. With i.p. implantation, values were −0.46 and −0.39 for i.v. and i.p. tracer injection, respectively. Figure 2 contains a comparison of the four regression equations relevant to this tumor and illustrates the parallel nature of the various lines. Intercept values for the four cases were distinct—being particularly small for the i.p. implantation examples. In the intraperitoneal case, the B values for the i.v. and i.p. injections were not significantly different.

DISCUSSION

Inverse correlations between tumor uptake and mass have been shown to be significant at the 1% level of confidence in 11 separate animal experiments. The largest correlation coefficients are found in nine of 11 cases using a power-law model. This relationship appears to be valid for three different types of tracers: stable vesicles, nonspecific monoclonal and specific monoclonal antibodies. If we hypothesize equal probabilities for power-law and exponential regressions, the likelihood of the former being observed in nine of 11 examples is 0.028. Thus, at a 5% level of confidence, the power-law relationship is the most likely of the three linear regression models of Eq. (1).

Regression analysis may also be useful in checking the internal consistency of data. In the Hagan et al. (5) report, uptake of the nonspecific MAb, PSA-399 by the SC lymphoma was said to be unrelated to lesion mass. Power-law analysis of their total of 15 data points, however, revealed a correlation (−0.807) that is significant at the 0.1% level. Hagan et al. presumably referred to the two highlighted points in Figure 3 as indicative of the lack of a relationship. These two values are suspect since they indicate uptakes as high as or higher

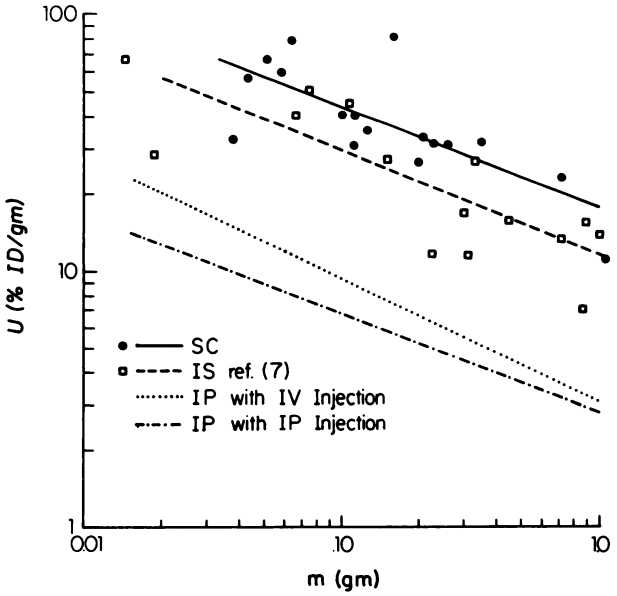

FIGURE 2
Four power-law regression lines obtained from experimental uptake data using the human LS174T tumor. Implantation was subcutaneous (SC), intrasplenic (IS), or intraperitoneal (IP). In the latter case, both IV and IP injections were possible; otherwise IV administration of the specific MAb was used. Because of the large number and scatter of IP tumor uptakes, only SC and IS implantation data are shown. Axes are logarithmic.

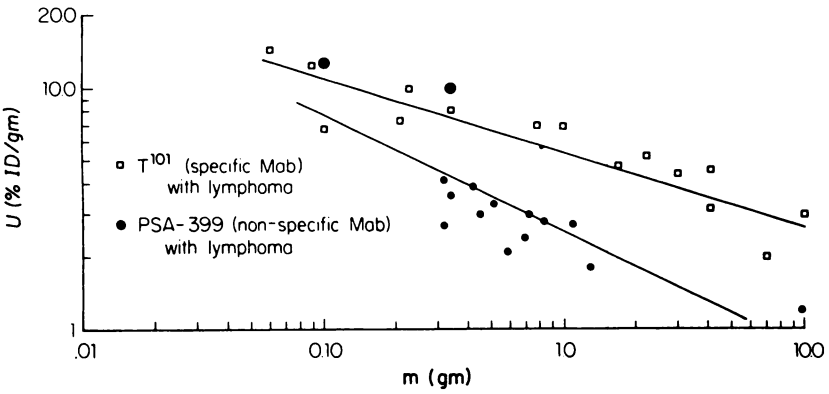

FIGURE 3
A comparison of nonspecific and specific MAb uptake in the lymphoma model. Data are from Reference 5 with the two suspect nonspecific points highlighted. If these are excluded from the analysis, the nonspecific power-law uptake curve becomes parallel to that of the specific case. Axes are logarithmic.

than the corresponding values obtained using a specific MAb on the same tumor model. If we omit these points, the power-law correlation improves to a value of −0.864, while the slope changes from −0.49 to −0.32. The latter exponent is more consistent with the value found with the lymphoma model and the specific MAb, T101 (cf. Table 2). We would suggest, therefore, that these two points may be incorrect and that they should be corroborated with future experiments.

An alternative explanation of these unusual values is the possibility of very large individual differences in tumor accumulation. Individual variations are clearly present in all experiments and are the probable dominant source of scatter about the least squares regression lines as shown in Figures 2 and 3. Biologic factors influencing the u(m) function could include the possibility that a spectrum of different geometries is exhibited by a given tumor in vivo. This is equivalent to a range for the A parameter instead of a single value as assumed in the mathematical derivation. Likewise, the density of accessible receptor sites (B value) may be dependent upon individual geometric growth patterns so as to constitute a second type of uncontrolled variation.

Simple models of tumor growth are in agreement with the regression analysis in that they lead to predictions of a power-law correlation between uptake and mass. If we average the Table 2 slope data, using weighting factors proportional to the degrees of freedom in each data set (n − 2), an average A value of −0.43 is obtained. This is approximately midway between the spherical and cylindrical predictions.

Our results have several implications in the general analysis of biodistributions. First the dependence upon size implies that tabulations of tumor uptake should explicitly contain reference to any mass relationship involved. Only in this way can one compare various tracer/tumor combinations in vivo. Secondly, one can perhaps understand the slope parameter (A) of the power-law model in terms of lesion geometry. In the case of the LS174T tumor, measured slopes were consistently independent of the implantation site with SC, IS and IP values being comparable.

Intercepts, however, reflect accessibility via the vascular system and showed a much greater range in the tabulated data. Using the B values for vesicle tracers of Table 2, one finds that the EMT6 neoplasm had an uptake three-fold greater than Lewis Lung Carcinoma in the mouse. If we consider only subcutaneous xenografts in nude mice, intercepts varied by approximately a factor of six in our analyses. We interpret these differences as being due to the relative density of targeting sites and perfusion of the various lesions. Accessibility of the IP-implanted tumors appeared to be particularly low and independent of the route of tracer injection.

Taken together, these results indicate that the geometry of tumor blood flow is a dominant constraint on tracer uptake. Earlier, Kjartansson (*17*) demonstrated, using plethysmography, a monotonic decrease of flow with rat sarcoma size. More recently, employing the method of Song and Levitt (*18*), Sands et al. (*19*) have found a reduction of uptake of iodinated BSA with increasing murine lymphoma (SL2) mass. They were unable to see any similar variation of Clouser tumor uptake with lesion size. This might then be offered as an explanation of the lack of inverse correlation between u and m seen by Shah et al. (*7*) using this tumor model and a specific MAb tracer. The Clouser tumor is one of those apparently rare lesions wherein flow is independent of size. Again, however, even in this exceptional case, the correlation of tumor blood flow and tracer uptake is apparent.

We wish to emphasize that liposomal uptakes are appreciable with B values comparable to the better monoclonal agents; e.g., a 15.6 being found in the case of the EMT6 murine tumor. Positive vesicle results obtained with the rat sarcoma model (*2*) are also striking although a direct comparison to mouse data is not possible. If we apply a standard correction involving the ratio of total body masses of the two species, the rat uptake should be scaled upward by a factor of approximately sixfold to be compared to that of the smaller animal. This would correspond to a mouse-equivalent uptake (B value) of essentially 30 for this nonspecific agent using ^{67}Ga as its radiolabel. While the correction

factor may be questioned, the very high uptake seen by Ogihara et al. (*2*) is a remarkable experimental result.

Therapeutic applications of these three types of agents are also strongly dependent on the results shown here. Since the radiation dose estimate in the MIRD formulation (*20*) is proportional to u, relatively smaller lesions will receive higher radiation doses than larger masses. If we assume an exponent of −0.33, an order of magnitude change in m implies a variation in dose of approximately a factor of 2.3 (the cube root of 10). Setting this exponent to −0.5, this variation becomes more than a factor of three, Conversely, if the form of the correlation and the size and hence mass of a lesion are both known, one could predict the tumor's uptake and hence dosimetry for that particular tracer/tumor combination. In addition, it would be expected that sections of the tumor adjacent to vascularized regions would have appreciably higher accumulations of tracer material. For short-range ionizing particles, this phenomenon would lead to relatively rapid spatial variation of radiation dose.

Variations of tumor uptake with mass also imply that lesions will exhibit a differential sensitivity to radionuclide therapy with poorly perfused volumes; e.g., necrotic zones, being the most radioresistant.The u parameter may still be used to represent this behavior if one measures the spatial variation of tracer uptake in excised tumors. Microdosimetry could then be performed with such generalized u functions. By the same argument, a uniformly perfused tumor, such as the Clouser, would likely obviate these difficulties and be more amenable to radiotherapy.

One can query whether the animal results shown are consistent with human data. It is important to realize that a given tumor of mass m in man would, to lowest order, demonstrate a much lower uptake (%ID/g) than the same-sized lesion in a smaller animal. We can expect u to scale approximately as the fraction of total blood volume directed to the tumor; i.e., as m/M with M being the species total mass. Since man is around three orders of magnitude heavier than murine or rat species, human tumor uptakes would be expected to be on the order of percent injected dose per kilogram. With this scaling factor in mind, effectively a reduction of the B parameter of Eq. (1C), however, one can still question whether tumors in man exhibit the uptake variation with mass (the A dependence) seen here in animal implantation experiments.

Unfortunately, clinical trials of the agents described here with surgical follow-up have not progressed sufficiently to permit answers to this question. It may be that in man and in the realm of tumor sizes beyond 10 grams, a region not explored in murine or rat studies, the correlations observed here do not occur. It does seem important that such measurements be made in order to assess the magnitude and hence the effectiveness of the radiation doses. In the case of adjuvant radiation therapy post-surgery involving masses less than several grams, one would anticipate that the smaller the residual tumor bulk, the larger and hence more effective the dose. This may, in fact, be an ideal clinical application of vesicle or MAb-mediated radiotherapy or MAb immunotherapy.

ACKNOWLEDGMENTS

This investigation was supported by NIH Research Grant Number CA33572 from the National Cancer Institute. The work was made possible in part by support from the James H. Daughdrill Research Fellowship (L.E.W.). Some of the Indium-111 used in these studies was donated by Hybritech Inc. of San Diego.

REFERENCES

1. Patel KR, Tin GW, Williams LE, et al. Biodistribution of phospholipid vesicles in mice bearing lewis lung carcinoma and granuloma. *J Nucl Med* 1985; 26:1048–1055.
2. Ogihara I, Kojima S, Jay M. Differential uptake of gallium-67-labeled liposomes between tumors and inflammatory lesions in rats. *J Nucl Med* 1986; 27:1300–1307.
3. Wallingford RH, Williams LE. Is stability a key parameter in the accumulation of phospholipid vesicles in tumors? *J Nucl Med* 1985; 26:1180–1185.
4. Philben VJ, Jakowatz JG, Beatty BG, et al. The effect of tumor CEA content and tumor size on tissue uptake of indium 111-labeled anti-CEA monoclonal antibody. *Cancer* 1986; 57:571–576.
5. Hagan PL, Halpern SE, Dillman RO, et al. Tumor size: effect on monoclonal antibody uptake in tumor models. *J Nucl Med* 1986; 27:422–427.
6. Moshakis V, McIlhenney, Raghavan D, et al. Localization of human tumor xenografts after IV administration of radiolabeled monoclonal antibodies. *Br J Cancer* 1981; 44:91–99.
7. Shah SA, Gallagher BM, Sands H. Radioimmunodetection of small human tumor xenografts in spleen of athymic mice by monoclonal antibodies. *Cancer Res* 1985; 45:5824–5829.
8. Gullino PM, Grantham FH. Studies on the exchange of fluids between host and tumor. II. The blood flow of hepatomas and other tumors in rats and mice. *J Natl Cancer Inst* 1961; 27:1465.
9. Peterson H-J, ed. Tumor blood flow compared with normal tissue blood flow in tumor blood circulation: angiogenesis, vascular morphology and blood flow of experimental and human tumors. Boca Raton FL, CRC Press Inc, 1979, pp 103–114.
10. Williams LE, Proffitt RT, Lovisatti L. Possible applications of phospholipid vesicles (liposomes) in diagnostic radiology. *J Nucl Med Allied Sci* 1984; 28:45–51.
11. Mauk MR, Gamble RC. Preparation of lipid vesicles containing high levels of entrapped radioactive cations. *Anal Biochem* 1979; 94:302–307.
12. Hwang KJ, Merriam JE, Beaumier PL, et al. Encapsulation with high efficiency, of radioactive metal ions in liposomes. *Biochim Biophys Acta* 1982; 716:101–

109.
13. Paxton RJ, Jakowatz JG, Beatty JD, et al. High-specific-activity In-111-labeled anticarcinoembryonic antigen monoclonal antibody: improved method for the synthesis of diethylenetriaminepentaacetic acid conjugates. *Cancer Res* 1985; 45:5694–5699.
14. Martin KW, Halpern SE. Studies in carcinoembryonic antigen production, secretion and kinetics in BALB/C mice and a nude mouse-human tumor model. *Cancer Res* 1984; 44:5475–5481.
15. Jakowatz JG, Beatty BG, Vlahos WG, et al. High-specific-activity In-111-labeled anticarcinoembryonic antigen monoclonal antibody:biodistribution and imaging in nude mice bearing human colon cancer xenografts. *Cancer Res* 1985; 45:5700–5706.
16. Hobbie RK. Intermediate physics for medicine and biology. New York: John Wiley and Sons, 1978: 99–104.
17. Kjartansson I. Tumor circulation. An experimental study in the rat with a comparison of different methods for estimation of tumor blood flow. *Acta Chir Scand Suppl* 1976; 471.
18. Song CW, Levitt SH. Effect of x-irradiation on vascularity of normal tissues and experimental tumor. *Radiology* 1970; 94:445–447.
19. Sands H, Shah SA, Gallagher BM. Vascular volume and permeability of human and murine tumors grown in athymic mice. *Cancer Lett* 1985; 27:15–21.
20. Loevinger R, Berman M. A schema for absorbed-dose calculations for biologically distributed radionuclides. MIRD Pamphlet No 1, *J Nucl Med* 9: Supplement No 1, 7–14, 1968.